JOURNAL OF SPACECRAFT AND ROCKETS
Vol. 31, No. 3, May–June 1994

Aerodynamically Blunt and Sharp Bodies

W. H. Mason* and Jaewoo Lee†
Virginia Polytechnic Institute and State University, Blacksburg, Virginia 24061

Computational fluid dynamics studies at supersonic and hypersonic speeds have resulted in an improved understanding of the meaning of aerodynamically, as opposed to geometrically, sharp and blunt shapes. An analytic investigation using Newtonian theory was conducted to support the computational results. Based on this work, a new criterion for the definition of an aerodynamically sharp shape is proposed. Defining the power-law shape to be the relevant gauge function, one can classify bodies with $n > 2/3$ as aerodynamically sharp, even though the initial body slope dr/dx is 90 deg. The paper describes the analysis that resulted in the new sharp and blunt shape criteria for aerodynamics.

Nomenclature

A = constant in power-law body equation defining fineness ratio
C_p = pressure coefficient
f = fineness ratio for the Sears-Haack body, Eq. (9)
l = length of the body in definition of von Kármán ogive and Sears-Haack body
n =exponent in power-law body definition, Eq. (1)
R =longitudinal radius of curvature, Eq. (2)
$R(0)$ =longitudinal curvature at $x = 0$, the leading-edge radius
$R_{K\text{-}O}$ =longitudinal radius of curvature for a von Kármán ogive
$R_{S\text{-}H}$ =longitudinal radius of curvature for a Sears-Haack body
r =body radius at a given x location
$r_{K\text{-}O}$ =body radius for a von Kármán ogive
$r_{S\text{-}H}$ =body radius for the Sears-Haack body
S =cross-sectional area
$S_{K\text{-}O}$ =cross-sectional area of the von Kármán ogive
s =arc length along the surface from the leading edge, $x = 0$
V =volume of Sears-Haack body
x =axial distance from leading edge
ζ =transformed independent variable for the Sears-Haack body, Eq. (7)
θ =body slope angle, $\tan^{-1}(dr/dx)$

Introduction

WHAT is meant by blunt and sharp? Intuitively it seems clear. A geometrically sharp body is defined to be one with a finite slope at the tip, the leading-edge radius is zero, and the point feels sharp. In practice it is extremely difficult to fabricate a perfectly sharp tip. Any manufacturing error results in a significant deviation from the design contour, and furthermore sharp edges are difficult to maintain because they are easily damaged (often causing injuries). At a more fundamental level, no shape can be made that is perfectly sharp on a molecular scale. There is always some bluntness.

Applied aerodynamicists frequently need to decide when a shape can be treated as sharp rather than blunt relative to a flowfield treated as a continuum. Practical limits in manufacturing accuracy and the maintenance of tolerances require a precise definition when fabricating leading edges. Given that some bluntness will exist, current definitions of sharp or blunt shapes lack precision. The results of a recent computational evaluation of minimum drag axisymmetric bodies at supersonic and hypersonic speeds[1] suggest the possibility of a difference between shapes that are geometrically sharp ($dr/dx \neq \infty$ at $x = 0$) and shapes that behave aerodynamically as if they are sharp.

Many theoretically derived supersonic and hypersonic minimum-drag axisymmetric shapes have a surprising property: the angle of the initial slope dr/dx is 90 deg. They are geometrically blunt. Eggers et al.[2] presented the modern derivation of this result using Newtonian theory and also a discussion of Newton's original solution of the problem. The exact result is closely approximated by a power-law body with an exponent n of 0.75. If centrifugal force effects are included in Newtonian theory, the minimum drag occurs for an exponent n of 0.66. Using an asymptotic analysis approach, Cole[3] also reached these conclusions. Von Kármán used slender-body theory to obtain the minimum-drag ogive of given length and base area at supersonic speeds.[4] That shape is also blunt.

The computational investigation[1] of minimum-drag bodies at supersonic and moderate hypersonic speeds (Mach 3–12) confirmed that the bodies with the lowest wave drag were geometrically blunt. Computationally, the minimum-drag power-law body exponent n was found to be approximately 0.7.

The blunt nose property of minimum-drag shapes required a close examination of the computational solution near the nose. Initially the procedure used in Ref. 1 was to compute the blunt body solution in the vicinity of the nose and then, downstream of the nose, use the space-marching approach over the rest of the body to obtain results economically. After the first series of calculations using this procedure, it was found unnecessary to use the blunt-body solution for each case. Instead, an unusual behavior of the numerical solutions was observed during the examination of the results in the vicinity of the nose to validate the integrity of the computational results. Rather than finding a classical blunt-body solution at the nose ($dC_p/ds = 0$), a very different character, as shown later, was observed.

This paper describes the details of the geometry and aerodynamics of low-drag axisymmetric bodies in the vicinity of the nose, or leading edge, at zero angle of attack for supersonic/hypersonic speeds. Numerical and analytical methods are used to obtain a new criterion for the definition of aerodynamically sharp shapes. A significant improvement in the understanding of the aerodynamics of nearly pointed shapes is obtained as a result of the study.

Geometrical Analysis

Consider the power-law shape

$$r = Ax^n \tag{1}$$

where the values of n of interest range from 0 to 1. If $n < 1$, the body slope angle at the nose $x = 0$ is 90 deg, and the body is blunt.

Received June 17, 1992; presented as Paper 92-2727 at the AIAA 10th Applied Aerodynamics Conference, Palo Alto, CA, June 22–24, 1992; revision received Nov. 24, 1992; accepted for publication Nov. 30, 1992.

*Associate Professor, Department of Aerospace and Ocean Engineering. Associate Fellow AIAA.
†Graduate Research Assistant, Department of Aerospace and Ocean Engineering; currently Senior Researcher, Agency for Defense Development, Republic of Korea. Member AIAA.

A value of $n = 1$ or greater produces a geometrically sharp nose. Using the general formula for the longitudinal radius of curvature R,

$$R(x) = \left[1+\left(\frac{dr}{dx}\right)^2\right]^{3/2} \Big/ \left(\frac{d^2r}{dx^2}\right) \tag{2}$$

the power-law body given by Eq. (1) has a longitudinal radius of curvature $R(x)$ of

$$R(x) = \frac{1}{|n(n-1)A|}\left[x^{2/3(2-n)} + (nA)^2 x^{(4/3n-2/3)}\right]^{3/2} \tag{3}$$

The value of the nose radius is found by taking the limit of Eq. (3) as $x \to 0$. The first term in the square bracket will vanish unless $n \geq 2$ (not of practical interest). The exponent of the second term controls the result for practical cases. The longitudinal radius of curvature at $x = 0$, which is the leading edge or nose radius, is thus:

n	$R(0)$
$> 1/2$	0
$= 1/2$	$A^2/2$
$< 1/2$	∞

Only one value of n produces a nonzero finite value for the leading-edge radius. Traditional airfoil shapes are parabolic near the nose, the leading term in the definition of the shape is $x^{1/2}$, and they have finite values of the leading-edge radius. The power-law bodies that have minimum drag, $n = 0.7$, in fact have a zero leading-edge radius, even though they are geometrically blunt.

Shapes that have a zero nose radius, yet have an initial slope angle of 90 deg, are difficult to visualize. Figure 1 shows, as an example, the nose region of the 3/4 power-law body with a circle of radius $R_{circ}/L = 0.0004$ inscribed tangent to the 45-deg slope point on the power-law body. Note the extremely small scale of the figure. No matter how small, any circular arc with a finite radius fails to produce an accurate representation of the nose. Figure 2 provides examples of curvature distributions near the nose for three power-law bodies representing the three different cases of limiting behavior. The difference in the behavior of the different cases as $x \to 0$ is clear.

The power-law shape arises from hypersonic theory (in fact at the limit as $M \to \infty$). Another class of minimum-drag shapes is

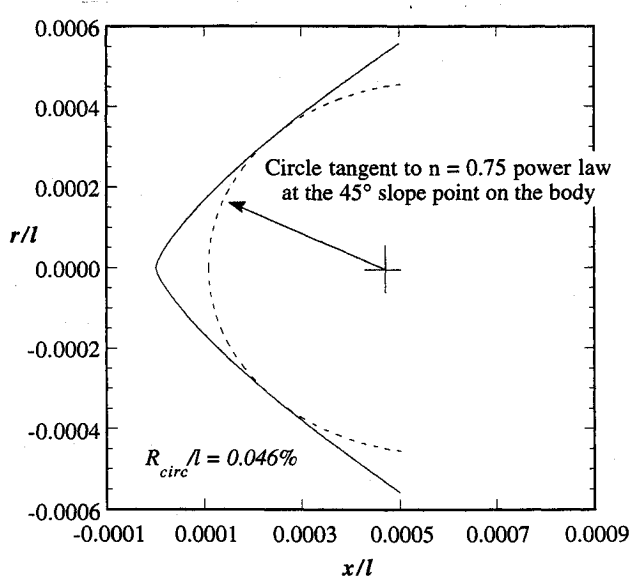

Fig. 1 Comparison of power-law body ($n = 0.75$) with inscribed circle near the leading edge.

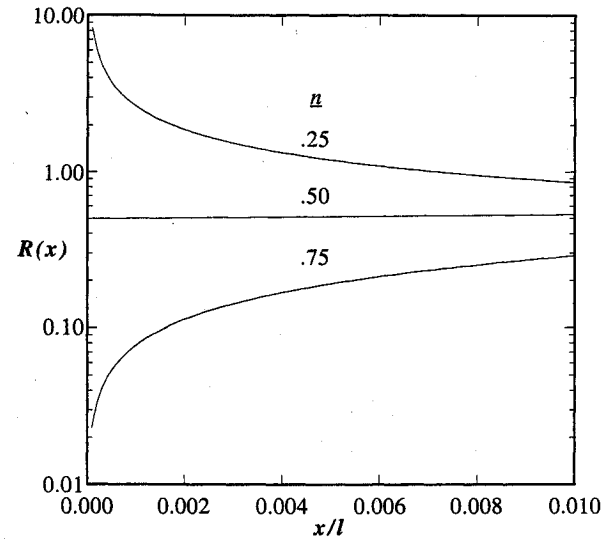

Fig. 2 Curvature distribution near the nose for various power-law bodies.

also of interest. Based on slender-body theory, the von Kármán ogive and Sears-Haack body are the lower supersonic Mach number equivalents to the power-law body for hypersonic flow. These bodies are also known to be slightly blunt at the tip. After the power-law shapes were examined, it became clear that the geometrical features of supersonic minimum-drag bodies should also be examined to determine if they showed similar unusual geometric characteristics.

The von Kármán ogive[4] is defined by

$$S_{K\text{-}O} = \pi r^2 = \frac{S(l)}{\pi}\left[\pi - \cos^{-1}\left(2\frac{x}{l}-1\right) + 2\left(2\frac{x}{l}-1\right)\sqrt{\frac{x}{l}\left(1-\frac{x}{l}\right)}\right] \tag{4}$$

and the longitudinal radius of curvature is

$$R_{K\text{-}O}(x) = 2\sqrt{\pi}\left[S_{K\text{-}O} + \left(\frac{1}{4\pi}\right)\left(\frac{dS_{K\text{-}O}}{dx}\right)^2\right]^{3/2} \times \left[S_{K\text{-}O}\left(\frac{d^2S_{K\text{-}O}}{dx^2}\right) - \frac{1}{2}\left(\frac{dS_{K\text{-}O}}{dx}\right)^2\right] \tag{5}$$

Similarly, the Sears-Haack body[4] is given by

$$\frac{r_{S\text{-}H}}{l} = \frac{1}{2f}(1-\varsigma^2)^{3/4} \tag{6}$$

where

$$\varsigma = 1 - 2\frac{x}{l} \tag{7}$$

The longitudinal radius of curvature becomes:

$$R_{S\text{-}H}(x) = \frac{2f}{3}\frac{(1-\varsigma^2)^{1/2}}{2-\varsigma^2}\left[(1-\varsigma^2)^{1/2} + \frac{9\varsigma^2}{4f^2}\right]^{3/2} \tag{8}$$

where f is related to the length and volume V by,

$$f = \sqrt{\frac{3\pi^2 l^3}{64\, V}} \tag{9}$$

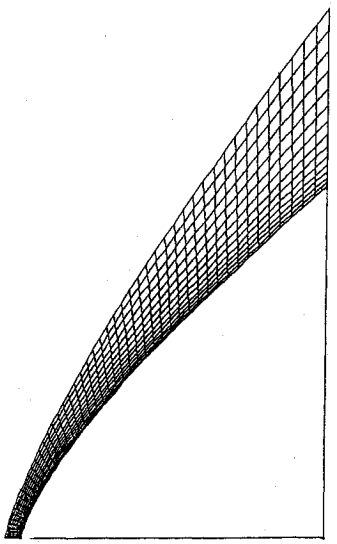

Fig. 3 Grid used for computations near the nose.

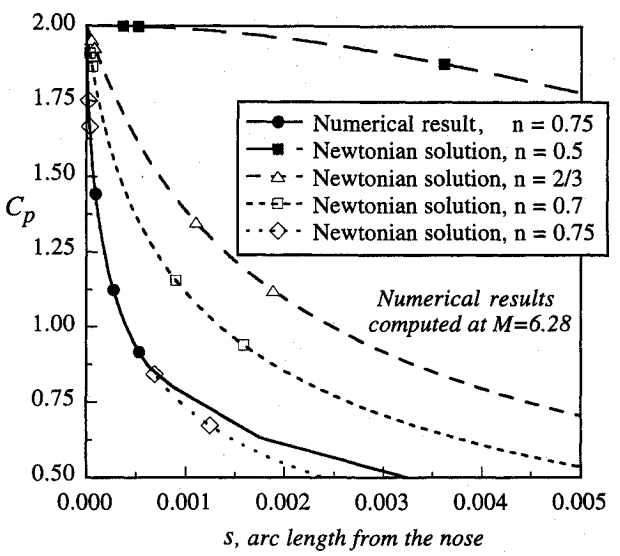

Fig. 4 CFL3DE and Newtonian solutions for power-law bodies plotted along the surface.

For both the von Kármán ogive and Sears-Haack body it was found from $R(x)$, using Eqs. (5) and (8), that the leading-edge radius was zero. Once this was discovered, the flowfield behavior near the nose was examined in more detail. This was done by determining the proper gauge function,[5] such that the ratio of the shape of the Sears-Haack body or von Kármán ogive to the gauge function remained finite as $x \to 0$. The power-law body was picked as a candidate gauge function, with an arbitrary value of the power-law exponent n. Thus the following relation was defined:

$$\lim_{x \to 0} \frac{r_{S\text{-}H} \text{ or } r_{K\text{-}O}}{Ax^n} = \text{const} \neq 0 \tag{10}$$

and an analysis was performed to find the value of n required to satisfy the relation.

The results of the analysis were that both the von Kármán ogive and the Sears-Haack body behave near the nose as a power-law body with $n = 3/4$, the same value as one of the theoretically derived minimum drag cases at hypersonic speeds. When $n = 3/4$,

$$r_{K\text{-}O} = \mathcal{O}(r_{\text{power-law body}})$$
$$r_{S\text{-}H} = \mathcal{O}(r_{\text{power-law body}}) \quad \text{as} \quad x \to 0 \tag{11}$$

Further analysis confirms that not only do the von Kármán ogive and Sears-Haack body behave similarly to the three-fourths power-law body, but also that the radius of curvature distribution near the nose is described by the three-fourths power-law body gauge function. When $n = 3/4$,

$$R_{K\text{-}O} = \mathcal{O}(R_{\text{power-law body}})$$
$$R_{S\text{-}H} = \mathcal{O}(R_{\text{power-law body}}) \quad \text{as} \quad x \to 0 \tag{12}$$

Thus, there is a direct and heretofore unsuspected similarity between the classical minimum-drag supersonic and hypersonic shapes. The geometry at the nose is the same in both cases.

Aerodynamic Analysis

The motivation for the present investigation originated during the examination of numerical solutions for the power-law bodies described in the vicinity of the nose. As noted earlier, it was expected that classical blunt-body pressure distributions would be observed, with the initial pressure gradient $dC_p/ds = 0$. Instead, solutions with very large initial pressure gradients were obtained. Because of the interest in accurate solutions for drag, this characteristic was closely examined.

The computational fluid dynamics method known as CFL3DE (Ref. 6) was used to make the computations. This code handles both calorically perfect and equilibrium air gas models and can be used to solve either the Euler equations or the thin-layer Navier-Stokes equations. Either space-marching or global iteration numerical techniques can be used. The present calculations used the Euler equations and the perfect-gas model. The method is a cell-centered finite volume scheme that uses upwind/relaxation methods and has been validated by numerous comparisons with data.[6] To investigate the detailed aerodynamic behavior near the nose, we used very dense grids. Fifty-one axial grid points were used along the first 0.04% of the body length. Between the body and the outer edge of the grid 20 points were used, with clustering near the body. In this method the shock is captured, and the grid was adjusted such that the detached shock was located approximately three-fourths of the way between the body and outer edge of the grid. Symmetric boundary conditions ($w = -w$ and $v = -v$, where v and w are the velocity components in the y and z directions) were used along the axial direction just at the nose. On the body surface the flow tangency condition was used. Freestream conditions were used on the outer boundary. The calculation was carried out in the axial direction far enough to insure that the flowfield was entirely supersonic at the downstream boundary. In this study of axisym-

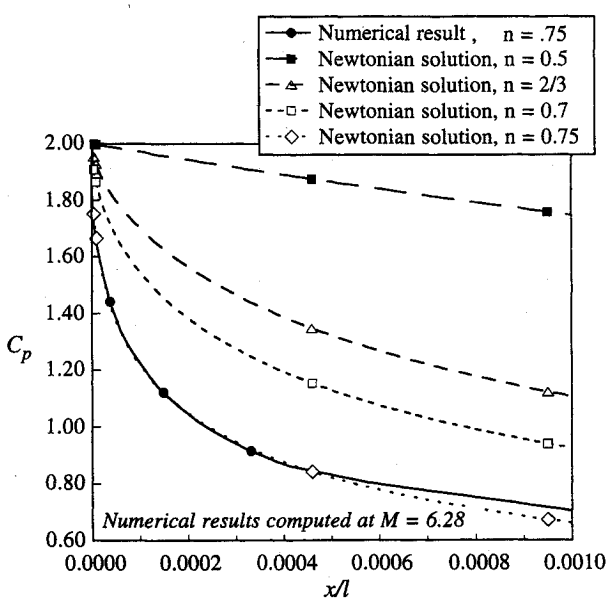

Fig. 5 CFL3DE and Newtonian solutions for power-law bodies, plotted along the axis.

metric bodies, CFL3DE was run using only one "slice" of the full three-dimensional grid in the circumferential direction and enforcing a boundary condition of no circumferential flow gradients. Figure 3 provides an example of the grid used in the calculations.

In addition to the examination of the numerical results, the pressure distribution was computed using Newtonian flow theory. CFL3DE results for the pressure coefficient for an $n = 0.75$ power-law body at a freestream Mach number of 6.28 and Newtonian solutions for several values of power-law index n are shown in Fig. 4 as a function of arc length s and in Fig. 5 as a function of axial distance x. The remarkably good agreement between CFL3DE and the Newtonian solution for $n = 0.75$ confirmed the surprising computational result that the initial pressure gradient for the flow is not zero and quite large. For $n = 0.5$, Fig. 4 shows the classical blunt-body pressure distribution originally expected.[7] The results show a natural progression from $n = 3/4$ to 1/2. The entire character of the pressure distribution changes between power-law bodies with $n =$ 1/2 and 2/3. Thus, the $n = 1/2$ value corresponds to an aerodynamically blunt body, whereas the $n = 2/3$ pressure distribution is characteristic of an aerodynamically sharp body.

To investigate this behavior further, we obtained an explicit relation for dC_p/ds for power-law shapes assuming Newtonian flow. Using Newtonian theory, we can give the pressure coefficient on the body surface by

$$C_p = 2 \sin^2\theta \tag{13}$$

where

$$\theta = \tan^{-1}\left(\frac{dx}{dr}\right) \tag{14}$$

Using these relations, we found that the pressure gradient along the arc length from the stagnation point is

$$\frac{dC_p}{ds} = -\left[\frac{4(1-n)}{A^3 n^3}\right] \frac{x^{(2-3n)}}{[1 + A^{-2} n^{-2} x^{2(1-n)}]^{5/2}} \tag{15}$$

Using Eq. (15), and investigating the limit as $x \to 0$, we found three distinct classes of results for the stagnation point pressure gradient, depending on the value of n:

n	$\left(\frac{dC_p}{ds}\right)$
$> 2/3$	$-\infty$
$= 2/3$	$-9(2A^3)$
$< 2/3$	0

This result is analogous to the result obtained in the analysis of the geometry, although there is a difference. In the geometry case, the critical value of the power-law exponent n was 1/2 as opposed to 2/3. Thus there is a region for power-law bodies, $1/2 < n < 2/3$, where the body has a zero leading-edge radius, but the pressure distribution at the leading edge continues to behave as if it were a blunt body.

In Fig. 6, the pressure gradients are shown as a function of arc length for several power-law indices n for a body with a fineness ratio of three ($A = 1/6$). As shown earlier, the Newtonian solution has an infinite pressure gradient exactly at the nose if $n > 2/3$. The singularity is $\mathcal{O}[s^{(2-3n)/n}]$. For $n = 3/4$, the singularity is $\mathcal{O}(s^{-1/3})$ for dC_p/ds, where s is the arc length from the stagnation point.

The variation in pressure gradient shown in Fig. 6 is examined from another viewpoint in Fig. 7. Here the variation in pressure gradient is compared for various power-law body shapes from $n =$ 0.5 to 1.0 at different locations downstream from the nose. Each curve is normalized by its maximum value. The maximum value of the pressure gradient at $s/l = 0.1 \times 10^{-6}$ is -0.135×10^7, whereas the maximum value at $s/l = 0.1 \times 10^{-2}$ is -0.393×10^3. Thus there is a large variation. Very near the nose, the pressure gradient is small until $n = 0.72$, when it starts to increase dramatically.

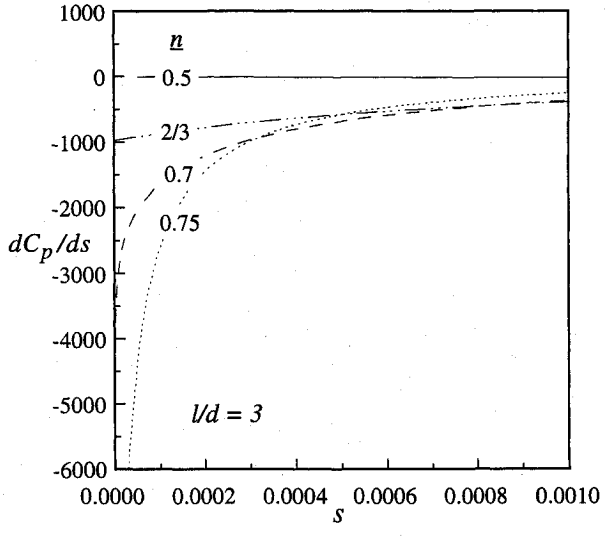

Fig. 6 Newtonian solution for the pressure gradient for power-law bodies.

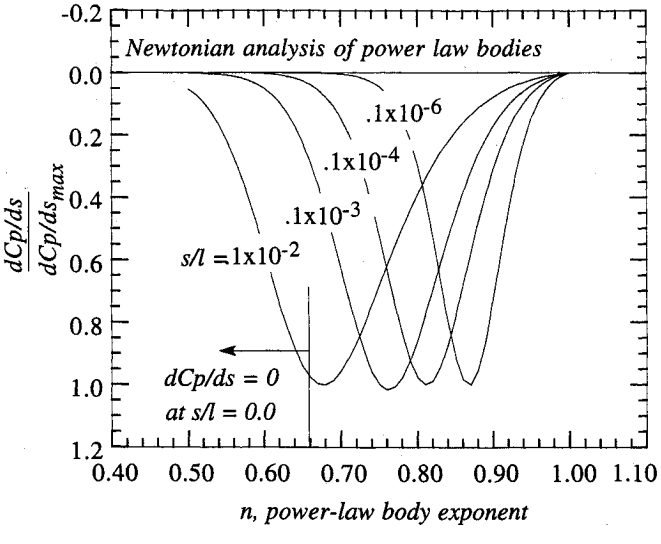

Fig. 7 Effect of power-law exponent on pressure gradient at different downstream locations.

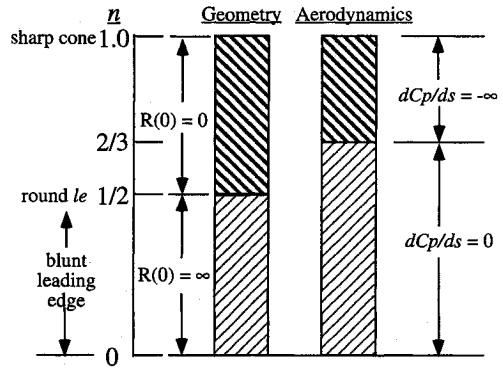

Fig. 8 Key regions for power-law body characteristics.

Thus, the use of minimum-drag shapes $n = 0.7$ does not result in initially huge pressure gradients.

Blunt and Sharp Nose Criteria and Nose Shaping

Based on geometric and aerodynamic analysis, it was shown that a class of body shapes exists for which the noses are geometrically blunt but for which the leading-edge radius is zero. Furthermore, there is a range of shapes where the flowfield solution is completely different from the classical blunt-body result, even though the tip has an initial slope of 90 deg. Considering power-law bodies, when $n > 1/2$, the leading-edge radius is zero. When $n > 2/3$, the shape produces a flowfield that does not exhibit classical blunt-body behavior and can be treated as if it were sharp for the calculation of the pressure distribution. Under these circumstances, space marching was found to provide an accurate pressure distribution, as shown in Ref. 1. Thus, any shape that has a power-law body gauge function is defined as an aerodynamically sharp shape when the power-law exponent n is greater than 2/3. Bodies being fabricated to meet an aerodynamically sharp requirement need only be fabricated to achieve this contour, not to obtain true geometric sharpness.

The results obtained are summarized in Fig. 8. Here the geometrical and aerodynamic analyses are compared schematically. The geometric boundary is precise. The aerodynamic boundary is based on Newtonian theory. However, the good agreement with CFL3D for the $n = 0.75$ case suggests that the aerodynamic boundary is likely to be very close to a boundary found from a more detailed numerical investigation. A numerical study to find a more precise boundary was not made.

Finally, one of the important aspects of the problem, the heat transfer, has not been considered. A fundamental advantage in using a blunt body is the substantial reduction of aerodynamic heating at the stagnation point, although low-drag, aerodynamically sharp noses will exhibit high values of heat transfer, even though the tip is blunt because of the large stagnation point velocity gradient. An approach to finding minimum-drag shapes subject to maximum limits for stagnation point heating was recently presented by Maestrello and Ting.[8]

Conclusions

Aerodynamically sharp shapes are different from geometrically sharp shapes. For axisymmetric bodies at supersonic and hypersonic speeds, the present analysis provides a means for distinguishing between aerodynamic sharpness and bluntness using the power-law shape as a gauge function. As shown using both Newtonian theory and a numerical investigation of the blunt noses on minimum-drag bodies, the new criterion for the definition of an aerodynamically sharp shape is as follows:

An axisymmetric body is aerodynamically sharp when the leading-edge geometry behaves as x^n where $n > 2/3$. Thus, an aerodynamically sharp shape is a shape that is $\mathcal{O}(x^n)$, $n > 2/3$. Under this criteria, the minimum-drag power-law shapes behave as though they are aerodynamically sharp even though they are not geometrically sharp.

Other related findings are the following:

Classical hypersonic and supersonic minimum-drag shapes are connected. The minimum-drag supersonic shapes based on slender-body theory (von Kármán ogive and Sears-Haack body) are also aerodynamically sharp using this criterion. They are $\mathcal{O}(x^{3/4})$ near the nose, which is the same as the classical power-law shape Newtonian theory minima for hypersonic flow. Supersonic slender-body theory and nonlinear hypersonic minimum-drag shapes both have the same shape at the nose.

The issue of "how sharp is sharp?" when considering the specification of contours for model and full-scale fabrication and manufacturing has been resolved. Aerodynamically sharp shapes do not have to be geometrically sharp.

These results provide an excellent example of how an examination of numerical solutions can lead to the re-examination of analytical theories to provide guidance and insight into aerodynamic phenomena.

Acknowledgment

We would like to acknowledge R. W. Walters of the Department of Aerospace and Ocean Engineering at the Virginia Polytechnic Institute and State University for providing us with access to CFL3DE and for consulting with us on the use of the code for this work.

References

[1]Mason, W. H., and Lee, J., "On Optimal Supersonic/Hypersonic Bodies," AIAA Paper 90-3072, Aug. 1990.

[2]Eggers, A. J., Jr., Resnikoff, M. M., and Dennis, D. D., "Bodies of Revolution Having Minimum-Drag at High Supersonic Speeds," NACA Rept. 1306, 1957.

[3]Cole, J. D., "Newtonian Flow Theory for Slender Bodies," *Journal of the Aerospace Sciences*, Vol. 24, No. 6, 1957, pp. 448–455.

[4]Ashley, H., and Landahl, M., *Aerodynamics of Wings and Bodies*, Addison-Wesley, Reading, MA, 1965, No. 6, pp. 178–181.

[5]Van Dyke, M., *Perturbation Methods in Fluid Mechanics*, annotated ed., Parabolic Press, Stanford, CA, 1975, pp. 23–26.

[6]Thomas, J. L., van Leer, B., and Walters, R. W., "Implicit Flux-Split Schemes for the Euler Equations," AIAA Paper 85-1680, July 1985.

[7]Anderson, J. D., Jr., *Hypersonic and High Temperature Gas Dynamics*, McGraw-Hill, New York, 1989, pp. 166–189.

[8]Maestrello, L., and Ting, L., "Optimum Shape of a Blunt Forebody in Hypersonic Flow," Inst. for Computer Applications in Science and Engineering, ICASE Rept. 89-51, Dec. 1989.

Jerry M. Allen
Associate Editor